PHYSICAL REVIEW MATERIALS **4**, 023402 (2020)

Window into NV center kinetics via repeated annealing and spatial tracking of thousands of individual NV centers

Srivatsa Chakravarthi,[1,*] Chris Moore,[2] April Opsvig,[1] Christian Pederson,[2] Emma Hunt,[2]
Andrew Ivanov,[2] Ian Christen,[2] Scott Dunham,[1] and Kai-Mei C. Fu[1,2]
[1] *Department of Electrical and Computer Engineering, University of Washington, Seattle, Washington 98195, USA*
[2] *Department of Physics, University of Washington, Seattle, Washington 98195, USA*

(Received 11 August 2019; accepted 24 December 2019; published 25 February 2020)

Knowledge of the nitrogen-vacancy (NV) center formation kinetics in diamond is critical to engineering sensors and quantum information devices based on this defect. Here we utilize the longitudinal tracking of single NV centers to elucidate NV defect kinetics during high-temperature annealing from 800–1100 °C in high-purity chemical-vapor-deposition diamond. We observe three phenomena which can coexist: NV formation, NV quenching, and NV orientation changes. Of relevance to NV-based applications, a 6- to 24-fold enhancement in the NV density, in the absence of sample irradiation, is observed by annealing at 980 °C, and NV orientation changes are observed at 1050 °C. With respect to the fundamental understanding of defect kinetics in ultrapure diamond, our results indicate a significant vacancy source can be activated for NV creation between 950–980 °C and suggest that native hydrogen from NVH_y complexes plays a dominant role in NV quenching, supported by recent *ab initio* calculations. Finally, the direct observation of orientation changes allows us to estimate an NV diffusion barrier of 4.7 ± 0.9 eV.

DOI: 10.1103/PhysRevMaterials.4.023402

I. INTRODUCTION

Nitrogen-vacancy centers in diamond are point defects that are utilized for sensing [1–3] and quantum information applications [4,5] due to their long spin coherence time [6] and optically accessible spin states [7]. Of significant interest are methods to synthesize negatively charged nitrogen-vacancy (NV^-) centers with minimal perturbation to the local environment, preserving the quantum and optical properties of the center. Full control over NV^- center formation requires a detailed understanding of all the underlying defect kinetics. While there has been progress in understanding NV^- center energetics [8–11] and engineering NV^- center formation kinetics [12], here we show how a new tool, the tracking of thousands of individual NV^- centers, lends insight into the formation, quenching, and orientation kinetics of a quantum defect in an ultrapure host.

We perform repeated vacuum annealing of chemical vapor deposition (CVD) diamond, and track individual NV^- centers between anneals via photoluminescence confocal microscopy on a large experimental volume ($350 \times 350 \times 25\,\mu\mathrm{m}^3$). We show a 6-fold to 24-fold sample- and location-dependent increase in the overall concentration of NV^- centers due to annealing at 980 °C. This indicates there is a source of vacancies within CVD diamond at moderate temperatures that enables one to significantly increase NV^- density without introducing additional lattice damage via irradiation. Individual NV^- tracking allows us to go beyond measuring simple net increases and decreases. Coincident with appearances, we are able to observe significant NV^- disappearances, with spikes in disappearances near 960 °C and 1050 °C. The disappearances near 960 °C would be completely masked by appearances in ensemble studies, but their presence provides an essential clue regarding the quenching process at higher temperatures.

At 1050 °C, we observe large-scale NV^- center orientation changes. After the first 1050 °C anneal, orientation changes are observed in the absence of a significant number of disappearances or appearances. Thus, only partial dissociation occurs at these temperatures. This lack of full dissociation indicates the observed disappearances at 960 °C and 1050 °C are not due to NV-disassociation but due to a quenching source (e.g., H). Finally, beginning at temperatures above 1000 °C, we begin to observe almost complete NV quenching originating from the surface.

II. EXPERIMENT

A. Samples

Our studies are performed on five commercial CVD samples (Element Six). Samples A, B, D, and E are "electronic grade" and have a substitutional nitrogen concentration of $[N_s] < 1$ ppb, according to the manufacturer. Sample C has $[N_s] < 1$ ppm. All samples have a {100} crystal orientation. Details of the growth conditions of the samples are not provided by Element Six, however, the growth temperature of similar samples is around 830 °C [13]. Prior studies of Element Six CVD diamond samples indicate a ratio of 1000 : 3 for $[N_s] : [NV^-]$ for {100}-oriented growth surfaces [14]. Using this ratio and confocal NV^- imaging, we estimate $[N_s]_{\mathrm{A,B,D,E}} \approx 1$ ppt in electronic grade samples and $[N_s]_{\mathrm{C}} \approx 50$ ppb in sample C (Table I).

---

[*] srivatsa@uw.edu

TABLE I. Summary of all samples with corresponding substitutional nitrogen, initial NV^-, and maximum NV^- densities. NV^- densities in samples A, B are estimated from the large-area scan data sets. For samples C to E densities are estimated from the depth scan data sets. Sample A, B, D, E densities are calculated from counting single NV^- centers in the confocal images and dividing by the scan volume (area × depth of focus). Details on the conversion are provided in the Supplemental Material [15]. Sample C density is estimated by normalizing the PL intensity to that of a single NV^- center and dividing by the confocal volume.

Sample	Initial $[N_s]$ estimate	Initial $[NV^-]_i$	Maximum $[NV^-]_{max}$	Enhancement $\frac{[NV^-]_{max}}{[NV^-]_i}$	Surface depletion	Orientation changes	Large scans	Depth scans
A[a]	0.8 ppt	2.3 ppq	2.7 ppq	1.2[b]	Yes	Yes	Yes	No
B	1.2 ppt	3.7 ppq	24.4 ppq	6.6	Yes	Yes	Yes	Yes
C	50 ppb	166 ppt	4 ppb	24.1	No	en[c]	No	Yes
D[d]	1.5 ppt	4.5 ppq	16.4 ppq	3.7	Yes	NA	No	Yes
E[d]	0.6 ppt	1.9 ppq	13.2 ppq	6.9	Yes	NA	No	Yes

[a] Sample underwent 2-hour anneals at 800 °C, 900 °C, 1000 °C, and 1100 °C.

[b] Enhancement not observed due to short annealing times and inhomogeneous surface driven depletion [15].

[c] Ensemble measurement, orientation changes are not distinguishable.

[d] Samples only annealed one time at 970 °C for 150 h.

B. Annealing

The diamond samples were annealed under vacuum (<1e-7 mbar) with anneals conducted in order of increasing temperature. A ramp time of 2 hours was used. To minimize surface fluorescence, the samples were cleaned for 90 minutes in a fuming acid bath (initial composition 1:1:1 H_2SO_4:HNO_3:$HClO_3$) maintained at 250 °C prior to annealing.

Sample A was annealed for 2 hours at temperatures 800 °C, 900 °C, 1000 °C, and 1100 °C and probed at 96 μm below the surface. In this dataset, a large number of NV^- appearances (25% of the total population) and disappearances (20%) were observed at 1000 °C. At 1100 °C, disappearances dominated with the total NV^- density depleted by more than 80% [15].

The sample A study motivated a finer temperature study from 950–1050 °C performed further from the surface. This full study was performed on sample B with annealing temperatures and times found in Table II. Due to the timescale of the observed processes, it was not feasible to reach thermal equilibrium at each temperature. Instead, the decision to increase the annealing time or annealing temperature was qualitatively based on the magnitude and/or saturation behavior of the observed changes. Annealing of sample C began at 980 °C to reproduce the NV^- appearances observed in sample B. Samples D and E were annealed only once at 970 °C.

C. NV identification and tracking

NV^- centers were imaged via confocal microscopy utilizing a 0.75 NA objective. The centers were nonresonantly excited with a linearly polarized 532-nm laser. The NV^- phonon sideband emission was filtered (660–800 nm) and detected with an avalanche photodiode. Further experimental details are provided in the Supplemental Material SM [15]. The excitation polarization angle was used to probe NV^- center orientation [14,16]. We can distinguish two sets of orientations, with two orientations in each set, in our {100}-oriented diamond samples. The two sets are indicated as green and magenta in Figs. 1 and 2. An automated stage with tandem micrometers and precision piezo-actuators enabled the generation of precise spatial maps of each NV^- center in the experimental area.

To characterize the outcome of each anneal, we performed two types of measurements: "large-area scans" and "depth scans," as illustrated in Fig. 1(c). Large-area scans longitudinally tracked individual NV^- centers in the same (350 × 350 μm^2) area at a depth of 240 μm (96 μm) from the top surface for sample B (A) with a depth-of-focus of 25 μm. The top surface is the surface closest to the microscope objective (SM [15]). Large-area scans captured both sets of NV^- orientations. Image registration, aided by persistent luminescent defects and local NV^- constellations, was performed to match

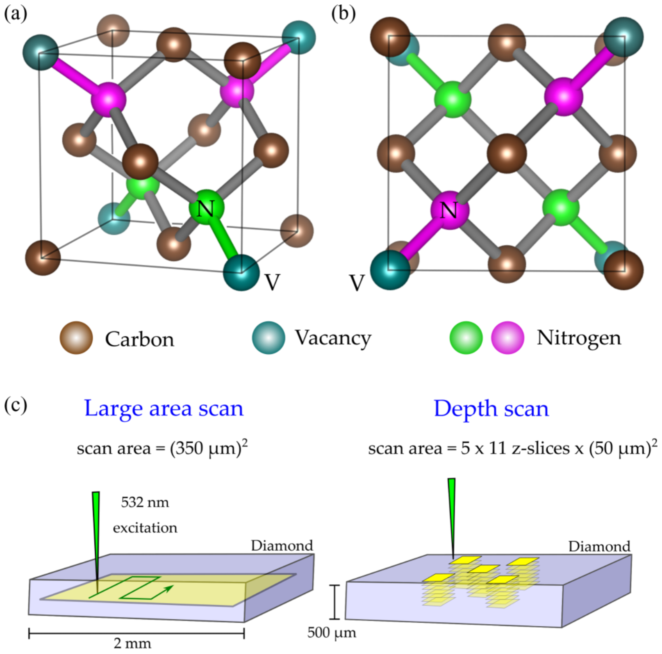

FIG. 1. The two optically distinguishable NV^- orientation sets are encoded in green and magenta. (a) Side view. (b) Top view. All surfaces are {100} planes. (c) Illustration of large-area scan and depth scan geometries.

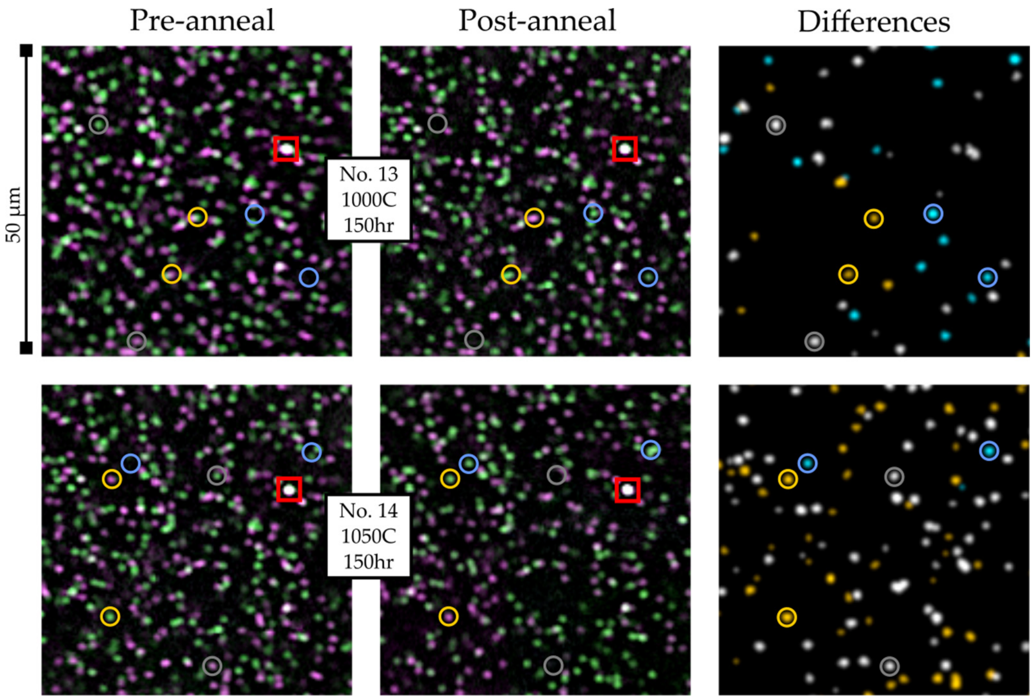

FIG. 2. A sequence of subareas of the "large-area scan" confocal images showing NV^- changes. Green and magenta indicate the two sets of distinguishable NV^- orientations. Two examples each of appearances, disappearances, and reorientations are indicated by blue, grey, and yellow circles, respectively. The red square marks a persistent defect used for image alignment.

individual NV^- center locations. The encoded NV^- orientation data provided additional information to confirm location and was utilized to identify orientation changes. The NV^- center appearances, disappearances, and orientation changes were obtained through image processing [17,18] and validated manually. Image processing details are provided in the Supplemental Material [15]. Examples of NV^- appearances, disappearances, and orientations in confocal images can be seen in Fig. 2.

Depth scans allow us to sample the NV^- density through the vertical cross-section of our diamond samples. A confocal scan ($50 \times 50\ \mu m^2$) was performed in five different regions in a quincunx pattern with 500-μm spacing. A single excitation polarization is used and depth scans do not track individual NV^- centers. For sample C, in which single NV^- centers could not be detected due to the high NV^- density, only depth scans were performed. Depth scans capture the NV^- density variation across and through the sample.

III. RESULTS

The results from both the large-area scans (sample A) and depth scans (samples A, B) are summarized in Figs. 3 and 4, respectively and in Table I.

A. Appearances

In sample B, we observe the NV^- center density increase during each anneal going from 950 °C to 980 °C (anneals 3–10 in Table II and Fig. 3). The continual observation of NV^- appearances motivated longer anneals (150 hours) starting at 980 °C (anneal 11) to observe saturation effects. A lower NV^- creation rate is indeed observed in the second 980 °C 150 hour anneal (anneal 12). A maximum 6-fold increase is observed after this anneal in the large-area scan data (pre-anneal versus anneal 12, Figs. 3 and S2 [15]), while the averaged data from the depth scans show a maximum 8-fold increase [pre-anneal versus anneal 15, Fig. 4(a)]. The variation in both density and density changes are attributed to the spatial variation of defect densities incorporated during the growth process. Average NV^- density varied by a factor of 3 across the five depth scan regions.

B. Disappearances

There are two different types of disappearance events: a spatially homogeneous NV^- depletion and a surface-driven inhomogeneous depletion. In sample B at 250-μm below the surface, we observe a small number of disappearances, homogeneously throughout the scan region, initially at every anneal temperature increment. We observe a larger number of disappearances at 960 °C and 1050 °C (Fig. 3). Very few disappearances are observed after the first 1050 °C anneal, suggesting the source of the quenching has been depleted. In the sample C ensemble measurements, we can also visibly observe a decrease in NV^- density during the first 1050 °C anneal [Fig. 4(c)].

A different behavior was observed at 1100 °C in sample A. At this temperature, we observed the majority of NV^- centers at a depth of 40 μm disappear. This surface-driven inhomogeneous depletion is also observed in sample B, as shown in Fig. 4(a); similar disappearances toward the surface begin to happen around $T \sim 980$ °C (anneal 10) and extend more that 100 microns into the surface by anneal 16.

TABLE II. Anneals conducted on samples B & C.

Anneal no.	1	2	3	4	5	6	7	8	9	10	11	12	13	14	15	16
Temperature, °C	800	800	950	960	960	970	970	970	980	980	980	980	1000	1050	1050	1050
Time, h	2	10	10	10	10	2	10	20	2	10	150	150	150	150	150	150
Sample	B	B	B	B	B	B	B	B	B	B	B,C	B,C	B,C	B,C	B,C	B,C

C. Orientation changes

Significant orientation changes are observed at 1050 °C. As shown in the sample B data (Fig. 3), the orientation changes are accompanied with an increase of disappearances during the first 1050 °C anneal. However, in subsequent 1050 °C anneals, orientation changes are not accompanied by a significant number of disappearances or appearances. Curiously, we observe a significant increase in orientation changes during subsequent 1050 °C anneal s.

IV. DISCUSSION

A. Appearances

We discuss three candidate processes for NV^- center appearances: charge state conversion of $NV^0 \rightarrow NV^-$, direct dissociation of $NVH \rightarrow NV + H$, and diffusion and capture of single vacancies, $N+V \rightarrow NV$. In high-purity type IIa diamond, both the neutral and negatively charged state of NV centers are stable under optical excitation. The ratio of the two populations at a given Fermi-level depends on the excitation wavelength and intensity [19,20]. In agreement with other groups studying high-purity CVD diamond with 532-nm excitation [21,22], we find NV^- is the dominant charge state [15] in pre- and post-annealed samples. If an NV is formed by the dissociation of a larger complex, the homogeneity and scale of NV^- appearances indicate this dissociating species should be uniform and abundant. In similar CVD samples, the NVH density is ten times greater than the NV^- density [14], suggesting NVH as the NV source. However, the dissociation of $NVH \rightarrow (NV + H)$ can be ruled out as this complex is observed to be stable until 1400 °C [23,24]. Single vacancies combining with native nitrogen is a third possible source. Single vacancies can exist in the neutral and negative (V^0 or V^-) charge states in diamond in which NV^- is the dominant NV charge state. It is generally accepted that vacancies are only mobile in their neutral charge (V^0) state at temperatures above 700 °C, with an activation energy of 2.3 eV [25]. However, it has been confirmed that the NV center forms as a unit during CVD growth [14,26] and not via vacancy capture. Thus during growth, all vacancies incorporated are either in the V^- state or trapped in complexes (V_2, NVH, VH, etc.). Divacancy (V_2) dissociation can be ruled out because it has been observed to anneal out at 800 °C [27] and other complexes have high ($>$1100 °C) dissociation temperatures. This leaves the negative vacancy (V^-). *Ab initio* calculations estimate a 3.4 eV migration energy for V^- [28]. Assuming a 30-THz attempt frequency, this migration energy corresponds to a diffusion length on the order of 100 nm for a 150-hour anneal at 980 °C. While there is uncertainty in both the migration energy and attempt frequency, direct migration and trapping of V^- appears to be a viable candidate for NV center formation. We note that NV formation in the absence of irradiation has previously been reported between 1500–1600 °C [26,29] in CVD diamond. The vacancy source in these reports could be similar to what we observe in our lower temperature, longer duration anneals, or could be due to dissociation of NVH [23,24] or VH [30].

B. Disappearances

The spatially homogeneous disappearances occur at temperatures below the full NV^- dissociation temperature (which our data show must be above 1050 °C), strongly suggesting

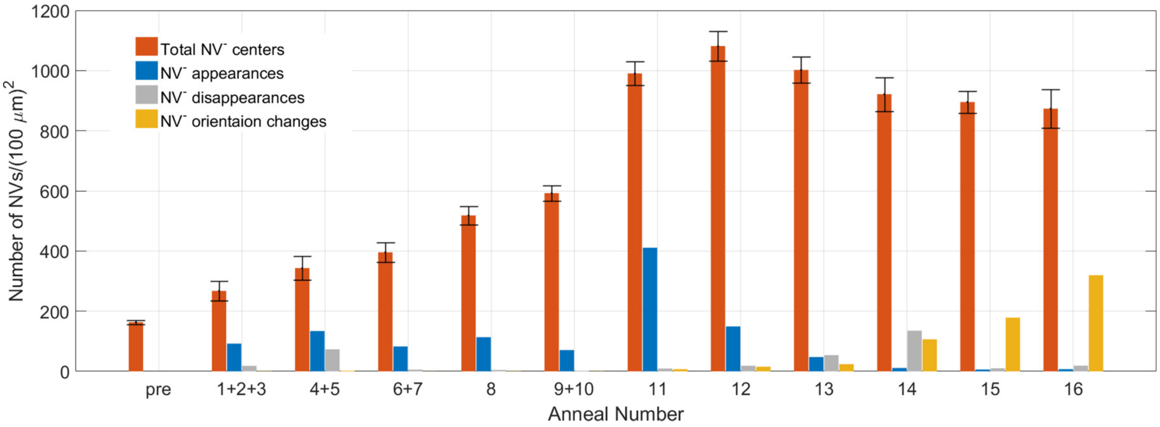

FIG. 3. Total NV^- density and observed changes obtained from the large-area scans ($\approx$350 $\times$350 μm^2) of sample B after every anneal. Several anneals are combined due to an inability to accurately match a significant portion of the scan area in the intermediate scans. For combined anneals, comparisons are made before and after the first and last anneals. Error bars represent uncertainty due to automation errors and differences in scan area between datasets [15]. Note the significant increase in annealing time which occurs at anneal 11.

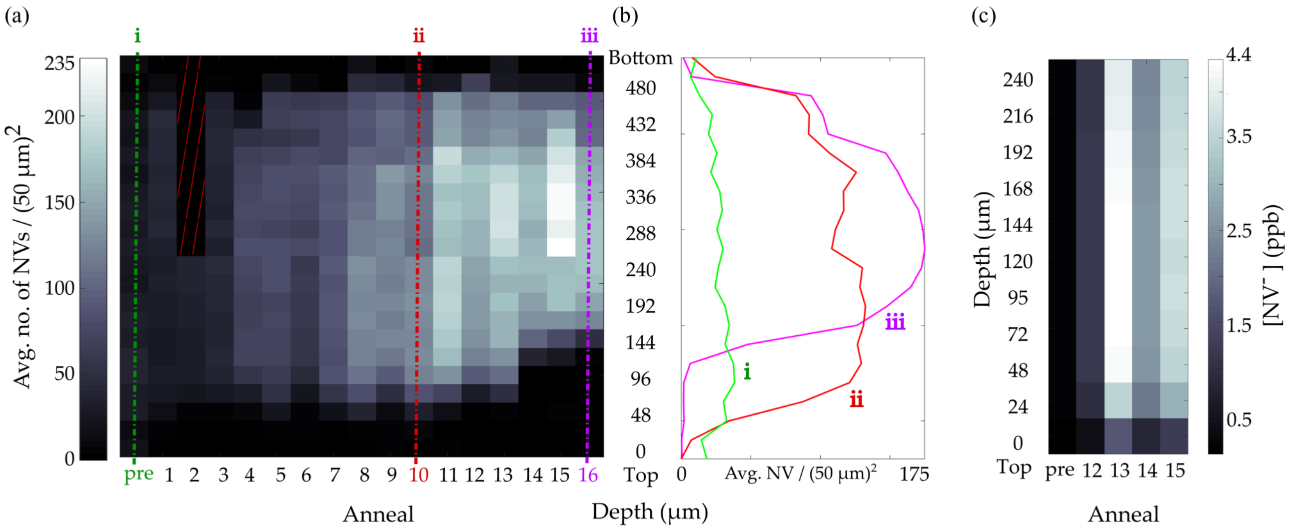

FIG. 4. (a) Plot of the average number of NV$^-$ centers per (50 μm)^2 area in sample B as a function of sample depth and anneal. To access the full depth profile with the limited piezo scan range, the sample is imaged from both the top and bottom surfaces. The two datasets are stitched at ~250 μm. The red hashed area indicates missing data. (b) Line plots of slices notated in (a). (c) Plot of NV$^-$ density in sample C as a function of sample depth and anneal.

another impurity is being trapped at the NV site. Hydrogen is the most likely candidate. Given the abundance of C, N, H, and vacancies in our samples, complexes either in the form of CH [31,32], NH [32], V_xH_y [24,33,34], or N_xVH_y [24,30,35] are potential spatially homogeneous hydrogen sources.

A comparison of our experimental results and recent *ab initio* calculations indicate the NVH_y complex, in which $y = 1, 2, 3$, is a plausible H source for the observed NV$^-$ quenching near 960 °C and 1050 °C. Salustro *et al.* [34] calculated the dissociation energies, E_H, for the following reaction path:

$$NVH_3 \xrightarrow[R_1]{E_H^1} NVH_2 + H \xrightarrow[R_2]{E_H^2} NVH + 2H \xrightarrow[R_3]{E_H^3} NV + 3H,$$

finding $E_H^1 = 2.83$ eV, $E_H^2 = 3.17$ eV, and $E_H^3 = 3.68$ eV. The dissociation rate for a given reaction is given by $R_i(T) = \nu_i \exp(-(E_H^i + E_D)/k_B T)$, in which T is the annealing temperature (in K), E_D is the dissociation barrier, and ν_i is the rate for capture of the H by the NVH complex. The ν_i primarily depend on the hopping rate for intersitial H and can be expected to be nearly the same for all the complexes. If we assume R_1 (the rate at which $NVH_3 \rightarrow NVH_2 + H$) becomes discernible at 960 °C (the temperature at which we first observe disappearances), we can estimate when R_2 become discernible using $R_2(T_2) \approx R_1(960\,^\circ\mathrm{C})$, finding $T_2 \approx 1110\,^\circ\mathrm{C}$. While this is higher than our observed second peak in disappearances at 1050 °C, we note that the 1050 °C anneal was more than seven times longer than the 960 °C anneal. Extrapolating further to the dissociation of NVH, we obtain that $R_3(1330\,^\circ\mathrm{C}) \approx R_1(960\,^\circ\mathrm{C})$. $T_3 = 1330\,^\circ\mathrm{C}$ is consistent with the experimental observation of NVH disappearance beginning near 1400 °C during shorter, 4-hour anneals [23,24].

We cannot use these annealing times to quantitatively predict when the ratios between R_1, R_2, and R_3 will become equal as disappearances typically saturate during each anneal. This saturation suggests a depletion of the H source. Qualitatively, however, the larger magnitude of disappearances at 1050 °C is consistent with a larger expected density [NVH_2] relative to [NVH_3].

In sample B, near-total NV depletion near the surfaces was observed starting at 980 °C [Fig. 4(b)], with the depletion layer growing in subsequent anneals. The surface dependence suggests a second, inhomogeneous, surface-driven hydrogen source. We believe this source is also the cause of the 80% depletion in sample A at 1100 °C [15], strongly suggesting large hydrogen diffusion length in diamond. The observation of a surface-driven depletion suggests it may be desirable to protect the diamond surface to preserve near-surface NV centers during annealing.

Both NV$^-$ PL quenching as well as enhancement has been reported in the literature over a wide range of temperatures from 1100–1500 °C [36–39], with higher temperature quenching often attributed to NV migration to form larger complexes [39,40]. Due to the short N_s diffusion length, complex formation with multiple N atoms (e.g., N_xVH_y, N_xV) can only explain quenching in high- N_s samples [29]. Our results indicate the following factors could contribute to the observed variance in NV quenching reported in the literature: (1) Compositional sample variance with respect to hydrogen traps; (2) Simultaneous creation and quenching events with the specific annealing temperatures and times determining a net outcome in either direction; and (3) the hydrogen content in the annealing furnace, suggested by our observed surface dependence of the depletion layer.

C. Orientation changes

Recently, a loss of preferential orientation was observed in ensembles of oriented NV centers [38] also at 1050 °C. The mechanism for this orientation change was believed to involve the full dissociation of the NV center with subsequent recombination with either the original N or another N in the lattice. Our single defect tracking shows that full dissociation does not occur at 1050 °C. If the vacancy is able to migrate, we would expect to observe orientation changes accompanied by NV^- disappearances. Additionally, if the vacancy diffusion length is comparable to the N_s-N_s spacing ($\sim 1\ \mu$m in sample B), we would also expect to see new NV^- appearances. However, after an initial round of disappearances in the first 1050 °C anneal, we primarily only observe orientation changes. This suggests there is an attractive force, extending to at least the third nearest neighbor (the minimum separation required for NV^- re-orientation), between the vacancy and the nitrogen [40]. While practical implementation may be challenging, this result opens a path toward preferential orientation by annealing under strain [41].

If many re-orientation cycles occur during a single anneal, we would statistically expect 50% of the NV^- centers will undergo a detectable orientation change. The maximum fraction of orientation changes we observe is 37% during anneal 16, suggesting that NV^- centers do not undergo multiple re-orientation cycles during each anneal. Thus, we can utilize the fractional rate from anneals 11–16 to estimate the orientation-change barrier E_b using the re-orientation rate $R = \nu \exp(-E_b/kT)$. A fit to the data gives $E_b = 4.7 \pm 0.9$ eV [15]. This value is comparable to the theoretical value of 4.85 eV [40] determined by density functional theory calculations. With a larger dataset and annealing times in which thermal equilibrium is reached for all processes, this method of observing orientation changes could be used to provide benchmarks for theoretical estimates of ν and E_b.

D. Comparison between samples B and C

Despite the almost five orders of magnitude difference in initial NV^- density between samples B and C, the spatially averaged results are qualitatively consistent, suggesting a similar interplay of defect species exists over a wide range of N doping. In both samples a large increase in the NV^- density is observed with long anneals at 980 °C and a decrease in NV^- density is observed at 1050 °C. While the results are qualitatively similar, quantitatively the magnitudes of the observed changes differ, suggesting the importance of the microscopic environment on the competing processes for defect formation. As we previously noted, variation in enhancement is observed even within a single sample. While beyond the scope of this work, future work could correlate annealing behavior with prior (NV^-, N_s, and NVH^-) density, appearances, or disappearances in this dataset [42] or future datasets.

V. CONCLUSION

The formation and dissociation of observable defects has long been used to probe defect kinetics in crystals. For example, a model for vacancy diffusion in diamond was facilitated by correlating V^0 (GR1) emission, V^- (ND1) absorption, and NV^- emission in ensembles of defects [25]. However, ensemble measurements such as photoluminescence, visible, and infrared absorption spectroscopy, and electron-spin resonance techniques, do not provide sufficient resolution and lack the sensitivity to probe competing mechanisms driving point defect kinetics (appearances versus disappearances; individual orientation changes). Nor do they typically have the sensitivity to probe ultrapure diamond samples with very low defect density (< parts-per-trillion) such as those now utilized for quantum information applications. Here we extend this ensemble technique using confocal microscopy, a tool capable of detecting single defects in bulk crystals. Two surprising results relevant to engineering NV centers for applications are obtained: (1) the observation of NV^- density enhancement in the absence of sample irradiation at 950–980 °C and (2) NV^- orientation changes in the absence of full NV dissociation at 1050 °C. Excitingly, the latter observation points to a route toward engineering the orientation of an NV^- center utilizing strain. Furthermore, NV quenching, which would be masked in the presence of NV formation in ensemble measurements, suggests NVH_x complexes are a likely candidate for the spatially homogeneous disappearances of NV centers at temperatures below 1050 °C. Thus we find that the longitudinal tracking of single NV^- centers through annealing is a promising tool for studying vacancy diffusion, hydrogen diffusion, the dissociation of hydrogen traps (e.g., NVH_x), and partial defect dissociation and re-orientation in ultrapure diamond.

ACKNOWLEDGMENTS

This material is based upon work supported by the National Science Foundation under Grants No. ECCS-180756 (primary for experiment) and No. DMR-1719797 (primary for theory). We thank undergraduates Brianna Birkel, Kelsey Bates, Phoenix Youngman, and Thalya Paleologu for assistance with the optical measurements; Mike Gould for assistance with annealing; and Matthew Markham for helpful discussions. Undergraduate student support for this project was provided under REU supplements to National Science Foundation Grants No. PHY-1150647, No. ECCS-1506473, No. EFMA-1640986, and No. PHY-1559631.

[1] L. Rondin, J.-P. Tetienne, T. Hingant, J.-F. Roch, P. Maletinsky, and V. Jacques, Rep. Prog. Phys. **77**, 056503 (2014).

[2] C. L. Degen, F. Reinhard, and P. Cappellaro, Rev. Mod. Phys. **89**, 035002 (2017).

[3] R. Schirhagl, K. Chang, M. Loretz, and C. L. Degen, Annu. Rev. Phys. Chem. **65**, 83 (2014).

[4] L. Childress and R. Hanson, MRS Bulletin **38**, 134 (2013).

[5] P. C. Humphreys, N. Kalb, J. P. J. Morits, R. N. Schouten, R. F. L. Vermeulen, D. J. Twitchen, M. Markham, and R. Hanson, Nature **558**, 268 (2018).

[6] G. Balasubramanian, P. Neumann, D. Twitchen, M. Markham, R. Kolesov, N. Mizuochi, J. Isoya, J. Achard, J. Beck, J. Tissler, V. Jacques, P. R. Hemmer, F. Jelezko, and J. Wrachtrup, Nat. Materials **8**, 383 (2009).

[7] M. W. Doherty, N. B. Manson, P. Delaney, F. Jelezko, J. Wrachtrup, and L. C. Hollenberg, Phys. Rep. **528**, 1 (2013).

[8] A. Mainwood, Phys. Rev. B **49**, 7934 (1994).

[9] J. P. Goss, P. R. Briddon, M. J. Rayson, S. J. Sque, and R. Jones, Phys. Rev. B **72**, 035214 (2005).

[10] P. Deák, B. Aradi, M. Kaviani, T. Frauenheim, and A. Gali, Phys. Rev. B **89**, 075203 (2014).

[11] D. Antonov, T. Häußermann, A. Aird, J. Roth, H.-R. Trebin, C. Müller, L. McGuinness, F. Jelezko, T. Yamamoto, J. Isoya, S. Pezzagna, J. Meijer, and J. Wrachtrup, Appl. Phys. Lett. **104**, 012105 (2014).

[12] F. Fávaro de Oliveira, D. Antonov, Y. Wang, P. Neumann, S. A. Momenzadeh, T. Häußermann, A. Pasquarelli, A. Denisenko, and J. Wrachtrup, Nat. Commun. **8**, 15409 (2017).

[13] J. Isberg, J. Hammersberg, E. Johansson, T. Wikström, D. J. Twitchen, A. J. Whitehead, S. E. Coe, and G. A. Scarsbrook, Science **297**, 1670 (2002).

[14] A. M. Edmonds, U. F. S. D'Haenens-Johansson, R. J. Cruddace, M. E. Newton, K.-M. C. Fu, C. Santori, R. G. Beausoleil, D. J. Twitchen, and M. L. Markham, Phys. Rev. B **86**, 035201 (2012).

[15] See Supplemental Material at http://link.aps.org/supplemental/10.1103/PhysRevMaterials.4.023402 for details regarding the experimental apparatus, data analysis techniques, sample variation, and additional supporting data.

[16] T. P. M. Alegre, C. Santori, G. Medeiros-Ribeiro, and R. G. Beausoleil, Phys. Rev. B **76**, 165205 (2007).

[17] C. T. Rueden, J. Schindelin, M. C. Hiner, B. E. DeZonia, A. E. Walter, E. T. Arena, and K. W. Eliceiri, BMC Bioinformatics **18**, 529 (2017).

[18] J. Schindelin, I. Arganda-Carreras, E. Frise, V. Kaynig, M. Longair, T. Pietzsch, S. Preibisch, C. Rueden, S. Saalfeld, B. Schmid, J.-Y. Tinevez, D. J. White, V. Hartenstein, K. Eliceiri, P. Tomancak, and A. Cardona, Nat. Methods **9**, 676 (2012).

[19] P. Siyushev, H. Pinto, M. Vörös, A. Gali, F. Jelezko, and J. Wrachtrup, Phys. Rev. Lett. **110**, 167402 (2013).

[20] N. Aslam, G. Waldherr, P. Neumann, F. Jelezko, and J. Wrachtrup, New J. Phys. **15**, 013064 (2013).

[21] S. T. Alsid, J. F. Barry, L. M. Pham, J. M. Schloss, M. F. O'Keeffe, P. Cappellaro, and D. A. Braje, Phys. Rev. Appl. **12**, 044003 (2019).

[22] X.-D. Chen, C.-L. Zou, F.-W. Sun, and G.-C. Guo, Appl. Phys. Lett. **103**, 013112 (2013).

[23] R. Cruddace, Magnetic resonance and optical studies of point defects in single crystal CVD diamond, Ph.D. thesis, University of Warwick, 2007.

[24] R. U. A. Khan, B. L. Cann, P. M. Martineau, J. Samartseva, J. J. P. Freeth, S. J. Sibley, C. B. Hartland, M. E. Newton, H. K. Dhillon, and D. J. Twitchen, J. Phys.: Condens. Matter **25**, 275801 (2013).

[25] G. Davies, S. C. Lawson, A. T. Collins, A. Mainwood, and S. J. Sharp, Phys. Rev. B **46**, 13157 (1992).

[26] C. Osterkamp, M. Mangold, J. Lang, P. Balasubramanian, T. Teraji, B. Naydenov, and F. Jelezko, Sci. Rep. **9**, 5786 (2019).

[27] D. J. Twitchen, M. E. Newton, J. M. Baker, T. R. Anthony, and W. F. Banholzer, Phys. Rev. B **59**, 12900 (1999).

[28] S. J. Breuer and P. R. Briddon, Phys. Rev. B **51**, 6984 (1995).

[29] T. Luhmann, N. Raatz, R. John, M. Lesik, J. Rodiger, M. Portail, D. Wildanger, F. Kleißler, K. Nordlund, A. Zaitsev, J.-F. Roch, A. Tallaire, J. Meijer, and S. Pezzagna, J. Phys. D: Appl. Phys. **51**, 483002 (2018).

[30] C. Glover, M. E. Newton, P. M. Martineau, S. Quinn, and D. J. Twitchen, Phys. Rev. Lett. **92**, 135502 (2004).

[31] F. Fuchs, C. Wild, K. Schwarz, W. Müller-Sebert, and P. Koidl, Appl. Phys. Lett. **66**, 177 (1995).

[32] J. P. Goss, R. Jones, M. I. Heggie, C. P. Ewels, P. R. Briddon, and S. Öberg, Phys. Rev. B **65**, 115207 (2002).

[33] S. Mehandru, A. B. Anderson, and J. C. Angus, J. Mater. Res. **7**, 689 (1992).

[34] S. Salustro, F. S. Gentile, A. Erba, P. Carbonniére, K. E. El-Kelany, and R. Dovesi, Carbon **132**, 210 (2018).

[35] S. Salustro, F. Gentile, P. D'Arco, B. Civalleri, M. Rérat, and R. Dovesi, Carbon **129**, 349 (2018).

[36] J.-P. Tetienne, R. W. de Gille, D. A. Broadway, T. Teraji, S. E. Lillie, J. M. McCoey, N. Dontschuk, L. T. Hall, A. Stacey, D. A. Simpson, and L. C. L. Hollenberg, Phys. Rev. B **97**, 085402 (2018).

[37] T. Yamamoto, T. Umeda, K. Watanabe, S. Onoda, M. L. Markham, D. J. Twitchen, B. Naydenov, L. P. McGuinness, T. Teraji, S. Koizumi, F. Dolde, H. Fedder, J. Honert, J. Wrachtrup, T. Ohshima, F. Jelezko, and J. Isoya, Phys. Rev. B **88**, 075206 (2013).

[38] H. Ozawa, H. Ishiwata, M. Hatano, and T. Iwasaki, Phys. Status Solidi (a) **215**, 1800342 (2018).

[39] S. Pezzagna, B. Naydenov, F. Jelezko, J. Wrachtrup, and J. Meijer, New J. Phys. **12**, 065017 (2010).

[40] H. Pinto, R. Jones, D. W. Palmer, J. P. Goss, P. R. Briddon, and S. Öberg, Phys. Status Solidi (a) **209**, 1765 (2012).

[41] T. Karin, S. Dunham, and K.-M. Fu, Appl. Phys. Lett. **105**, 053106 (2014).

[42] S. Chakravarthi, Full NV annealing dataset hosted under CC0 - Public Domain (Harvard Dataverse) (2019), doi:10.7910/DVN/V2EYN7.